



Porous Al₂O₃ Nanogeometry Sensor Films Growth and Analysis

W. G. Yelton,* K. B. Pfeifer,*^z and A. W. Staton

Sandia National Laboratories, Albuquerque, New Mexico 87185-1425, USA

Material studies of thin films of porous anodized Al₂O₃ have been undertaken to determine their applicability as sensing films for application on surface acoustic wave sensors. We describe the production of these films including their growth parameters and provide an analysis of their crystal morphology. These films were then exposed to various concentrations of analyte and their surface areas determined using Brunauer-Emmett-Teller-type analysis. Finally, the surface area as a function of anodization potential is provided for the films.

© 2001 The Electrochemical Society. [DOI: 10.1149/1.1421608] All rights reserved.

Manuscript submitted April 16, 2001; revised manuscript received September 6, 2001. Available electronically November 27, 2001.

Recent efforts have focused on the chemical and physical diversity of interface materials for surface acoustic wave (SAW) technology.¹ These materials provide SAW sensors with their analyte selectivity. Issues of wide dynamic range and high sensitivity must also be addressed for sensor arrays to compete in applications requiring low detection limits such as the development of sensor systems useful in the detection of chemical plumes for security applications. Each chemical sensor consists of interdigital transducers patterned on the surface of an ST-cut quartz substrate with a thin-film coating placed in the SAW propagation path to perturb the acoustic wave velocity during analyte sorption. Since no single coating provides absolute analyte specificity, an array of sensors provides a high degree of discrimination ability. By providing a diverse set of material coatings, the sensor array offers a degree of chemical sensitivity and selectivity. Because SAW devices respond in proportion to change in mass per nominal unit area of the device surface, sensitivity is enhanced by surface modification with high area, thin-film coating materials to allow a greater mass of analyte adsorption at a given ambient concentration. A number of anodization studies in the literature have dealt primarily with bulk materials and their resultant properties, which are significantly different from evaporative deposited thin-film systems.^{2,3} Other studies have dealt with the growth of porous alumina films formed on foil templates.⁴ This study deals with porous films grown *in situ* on a sensor substrate where the pore morphology and pore size is controlled by the substrate temperature and the anodization conditions.

Material studies of thin (<1 μm), high surface area, metal/oxide films developed to improve SAW sensitivity, reveal common factors that, in fact, diminish sensor sensitivity. These factors include non-uniformity in the density of the material, the rigidity of the microstructure, and nonuniformity in the thickness of the coating. For example, films developed from high density materials such as Pt, Pd, or Au, have yielded higher dendritic nanogeometries but suffer greater insertion losses for a given thickness. In contrast, because of its low density, microstructure rigidity, ordered porosity, and controllable pore volume, anodized aluminum (Al₂O₃) formed from evaporated deposition of metallic Al suggests promising films for enhanced sensor sensitivity. In the context of this paper, anodized aluminum and alumina refer to two different coatings. Anodized aluminum is a coating where only part of the evaporated aluminum has been converted to alumina. Under this oxidized layer remains metallic aluminum. For alumina, on the other hand, the evaporative aluminum film has been completely converted to an oxide, no additional aluminum is available for anodizing.

Experimental

Growth and deposition.—During physical evaporative depositions, the dominant influence on the final microstructure of an Al₂O₃ coating is strongly linked to the surface mobility of the adatoms, which is affected by the substrate temperature and deposition rate. The microstructure of evaporative films can be viewed in terms of the Movchan-Demchishin model also known as the zone structure model (ZSM).⁵ In this model, coatings are deposited under three distinct conditions or “zones.” At a constant evaporation rate, the material morphology in each zone can be manipulated by the temperature of the substrate (T_s) onto which the Al is deposited. Zones are classified as zone I ($T_s < 0.3T_m$), zone II ($0.3T_m < T_s < 0.45T_m$), and zone III ($T_s > 0.45T_m$) where T_m refers to the melting point of bulk Al.

In zone I, film growth is more agglomerated with “islands” of crystalline structures separated by small columnar voids. Because of low thermal energy, due in part to the relatively low substrate temperature as compared to the melting point of the material, the surface mobility of adatoms is limited. The image in Fig. 1 is a cross-sectional view of an agglomerated structure of alumina formed by the anodizing process of evaporated aluminum on a quartz substrate deposited under zone I conditions. After sulfuric acid (0.5 M) anodization under fixed (16 V) anodic potential, the crystal morphology of the Al₂O₃ in Fig. 1 is characterized by disordered alumina microstructures with low effective surface areas. From tunneling electron microscopy (TEM) analysis, these agglomerated oxides reveal tortuous pore openings with diameters on the same order as films developed under zone II conditions, but with limited pore length and corresponding limited pore volume. These features are not visible with high resolution scanning electron microscopy (SEM) examination.

Anodization.—Figure 2 is the cross section of an alumina film formed by the anodizing process of evaporated aluminum grown under zone II conditions. The initial film was vapor deposited under the same conditions as the film in Fig. 1, except that the substrate temperature was held at $0.4 T_m$. Under zone II conditions, film growth occurs with greater adatom mobility, and favors columnar grain structures with dense intercrystalline boundaries that extend through the coating thickness. The anodization conditions were identical for both films and consist of mounting an Al coated SAW device to a rigid Teflon fixture that was centered in a 250 mL beaker 1 cm from a Pt counter electrode. Electrical contact to the Al film was made through a 1 mm Ti wire mounted on the Teflon fixture. DC resistance was observed at the Ti wire tip (opposite the Ti/Al contact) and a point on the Al surface. If the resistance was $3 \Omega/\text{cm}^2$ or higher, the contact points were filed and cleaned and then the resistance was rechecked.

Prior to entering the solution, power was activated to the electrochemical cell. Before and during the anodizing process, N₂ gas was bubbled through the anodizing solution in front of the SAW

* Electrochemical Society Active Member.

^z E-mail: kbpfeif@sandia.gov

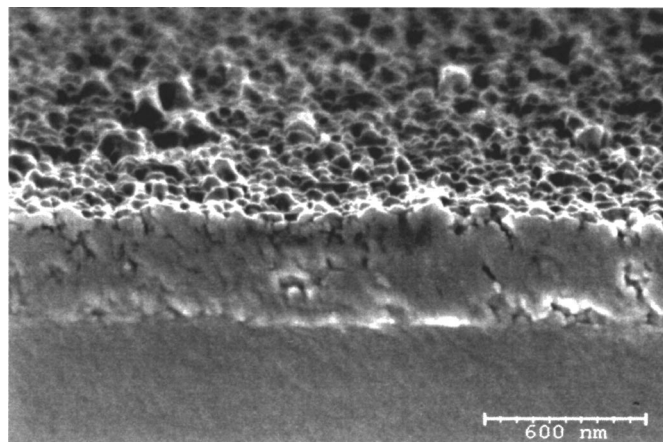


Figure 1. SEM cross section of an alumina film formed by anodizing (16 V applied) evaporated aluminum that was thermally evaporated on quartz at low temperature of 53°C substrate temperature ($0.08 T_m$). Because of low adatom mobility, the microstructure of the deposit is more agglomerated with voids.

device. The N_2 helped to agitate the solution, and for small surface areas, was sufficient for maintaining the temperature of the cell. The samples in Fig. 1 and 2 were anodized at a constant potential of 16 V. For all samples anodized at potentials from 2-25 V, we used 0.5 M H_2SO_4 as the electrolyte. Samples used for the adsorption study were prepared under zone II conditions and anodized for 40 min. These 500 nm films were completely converted to alumina. At these exposures, the finished film thickness ranged from 550-620 nm depending on the driving potential, with higher potentials yielding thicker films and larger pore diameters. Films anodized much longer (stage III) were thinner than the initial 500 nm seed layer with larger pore diameters for a given fixed potential, as compared to alumina films formed under identical conditions but for shorter anodizing times.

Figure 2 reveals straight ordered columns extending from the surface to the substrate. This scanning electron micrograph (SEM) is viewed using a 300 nm scale to clearly reveal the ordered columnar structure in contrast to Fig. 1, which is viewed from a slightly macroview (600 nm scale) to reveal the disorder surface as well as the cross-sectional structure.

The graph in Fig. 3 reflects the current decay over time as an aluminum film, formed under zone II evaporation, is anodized under constant potential. As the aluminum oxide forms, the surface resis-

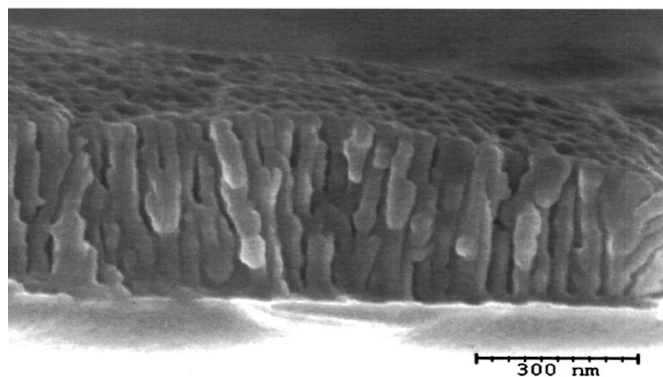


Figure 2. Fractured SEM cross section of an alumina film formed by anodizing (16 V applied) evaporated aluminum. The aluminum was thermally evaporated on quartz at 250°C substrate temperature ($0.4 T_m$). Due to increased adatom mobility, the microstructure of the deposit is more columnar with distinct intercrystalline boundaries.

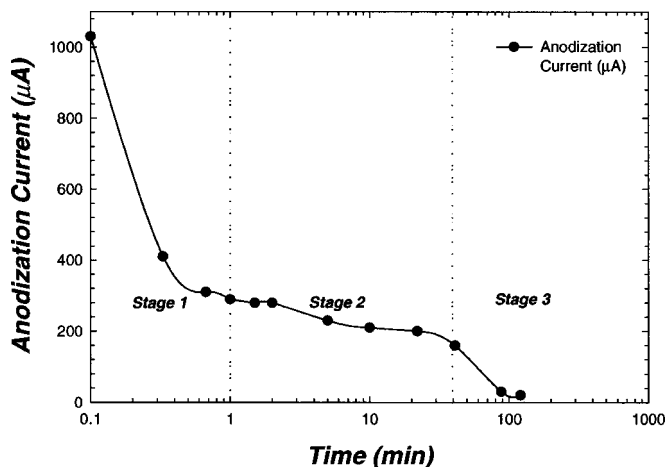


Figure 3. The current decay of 500 nm aluminum evaporated film during constant potential anodization. Solid line is a spline fit of the data as guide to the eye. Note that the current asymptotically approaches a constant value at the end of the stage 3 growth.

tance of the film increases dramatically. The solid line in Fig. 3 is a guide for the eye. The film undergoes three stages of change under potentiostatic mode. During the first (growth) stage (the first 60 s in this example), the current drops at a rapid rate, indicating that the nucleation of oxides and crystal structure ordering of the Al_2O_3 is occurring. During the second stage (see Fig. 4), SEM micrographs at 1, 3.5, and 10 min reveal the formation of the oxide with increasing depths as a function of time. From zone II deposition, the unanodized aluminum film evaporated on quartz appears quite rough with a number of large voids. After 60 s of anodization with an applied potential of 10 V, a uniform oxide of 100-150 nm consumes and covers the surface. At 3.5 min, more than 25% of the aluminum is consumed. When 10 min have passed, most of the available aluminum is gone.

As anodization time increases, the thickness of the oxide film grows, consuming and converting the aluminum underlying to an oxide. During stage II (see Fig. 3), the current is fairly stable and the general morphology of the crystal structure is now ordered and the remaining aluminum is converted to oxides by the slow diffusion of oxygen through the thicker oxide film above. During this second stage, the porous film reaches its highest level of impedance for a given overall thickness.

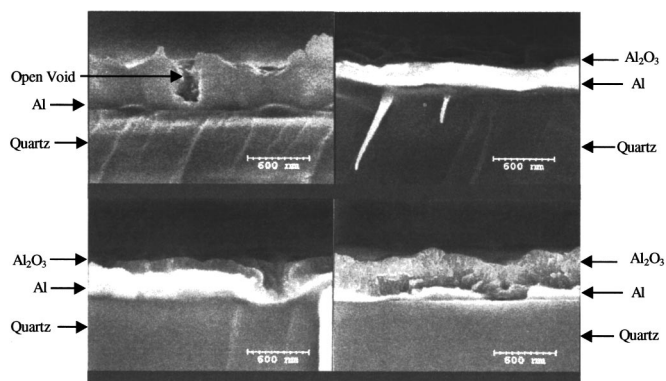


Figure 4. SEM cross sections of films that have been anodized for various times. The four images are viewed from samples that were fractured to reveal cross sections of aluminum oxide, aluminum, and the quartz substrate. The unanodized film is in the upper left-hand corner and proceeding clockwise the photographs are 1, 10, and 3.5 min. All films were deposited under zone II conditions and were anodized at a 10 V potential.

Table I. Table of pore diameter compared to applied potential and anodization time. Data was obtained from SEM micrographs that were near the resolution limit for the smaller pores. However, the general trend toward larger pores with larger applied potential is illustrated.

Applied potential (V)	Time (min)	Pore diameter (nm)
3	125	12 ± 2
10	1	7 ± 2
10	60	10 ± 2
10	200	17 ± 3
12	120	20 ± 5
16	120	30 ± 10

For a film of 500 nm thickness, when anodized at a potential of 10 V, the evaporated bulk aluminum was completely consumed after approximately 40 min corresponding to the observed drop in current illustrated in Fig. 3. During stage III (see Fig. 3), the elemental aluminum has been consumed and converted to oxides. SEM micrographs at 60 and 105 min (not shown) reveal discreet columnar ordering of the oxide down to the supporting quartz substrate.

Table I is a summary of the pore size data obtained from the experiment compared to the applied potential and anodization time. This data was obtained by measuring the pore sizes from SEM photos of the anodized films. Each measurement was obtained by making six to seven measurements from a level section of the coating while avoiding the grain boundaries. An attempt was made to pick points in clusters that represented the bulk surface finish. Since each surface has mountain and valley-like features, the measurements were made on flat mountain-like mesas. At these points, the low voltage (<10 V) formed oxides had similar pore sizes and very little variance. The limited variance in pore size measurements is the result of the SEM resolution. However, at larger voltages, larger pores were very clear and easily measurable. Table I illustrates the trend for larger pore size resulting from higher applied anodization potentials.

Figure 5 illustrates the surface of four aluminum films. The unanodized film, sanded at 600 nm, reveals large grain structures with two voids centered among the cluster of grain structures. Viewed at 200 nm, the surface is covered with pores within 60 s of the beginning of the anodization process. From the plane view after 60 min, the pores

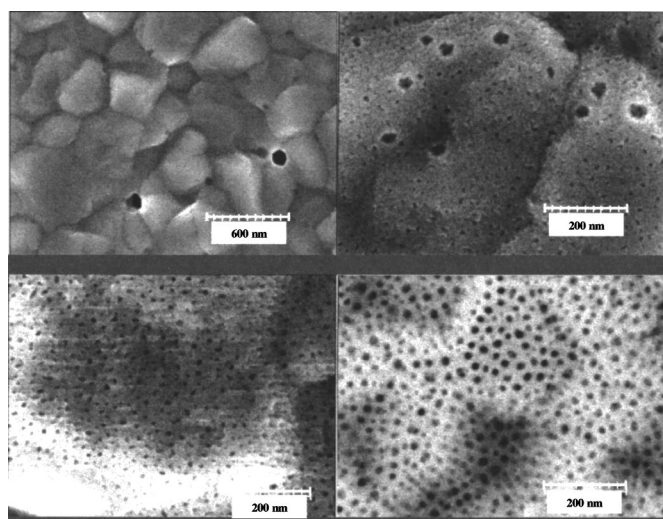


Figure 5. SEM photograph of Al_2O_3 surface as a function of anodization potential. Clockwise from the upper left-hand corner the films are unanodized, anodized for 1 min at 10 V, anodized for 200 min at 10 V, and anodized for 60 min at 10 V. These photos illustrate that after 60 min of anodization, the films are etched by the process and begin to open the pores.

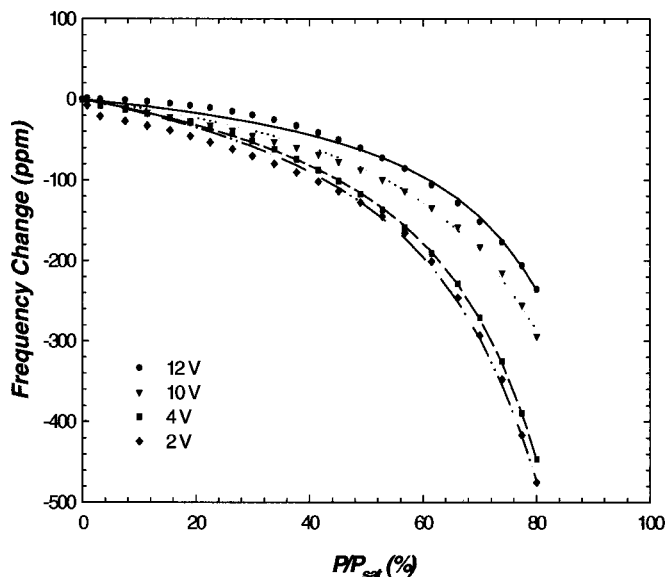


Figure 6. Plot of frequency change vs. concentration (P/P_{sat}) for EtOH on SAW devices with Al_2O_3 films produced by the described process. Each curve represents a different anodization voltage and the lines are modified BET fits to the data.

are uniformly spaced with uniform pore openings (*ca.* 10 nm). At 105 min (not shown), the pores remain fairly uniformly spaced but the pore openings at the surface begin to show signs of widening. From a cross-sectional view of this film, the columnar structures are showing signs of separation at the surface. In this final stage of the process, the current in Fig. 3 drops off at an accelerated rate. During this stage, the film is no longer highly conductive as when there was a source of electroactive aluminum available, and the acid electrolyte surrounding the film in the anodizing solution now acts as an etchant. As the film is continuously exposed to the acid electrolyte, the pores are widened and the film becomes thinner. Even though the supporting electrolyte is able to maintain a small flow of current between electrodes, the current is converging asymptotically to a constant value. In Fig. 5, the SEM micrograph of a film processed at 200 min reveals wider pore openings (*ca.* 20 nm), and a breakdown in structure uniformity, along with a thinner overall film thickness.

Analysis

A series of metallic Al films were vapor deposited (500 nm) on SAW devices and anodized at various applied potentials (2–12 V) for 40 to 60 min. The pore diameters measured from SEM micrographs for samples prepared at 2 V are *ca.* 7 nm, and for samples anodized at 12 V are *ca.* 20 nm. A fractured cross section of a film is shown in Fig. 4.

The functionality of these films as sensors was tested. Each SAW device was used as the feedback element of an oscillator circuit operating at approximately 97 MHz. The frequency outputs from the oscillators were then measured using a frequency counter. Figure 6 is the frequency shift of four SAW devices during the adsorption of ethanol at increasing normalized vapor pressures. Insertion losses for these coated devices were less than 1 dB greater than for a bare device, but film sensitivity increases were of an order of magnitude over a bare device. A decrease in pore size yielded an increase in sensitivity.

The modified adsorption model of Brunauer, Emmett, and Teller (BET)^{6,7} has been applied to the problem of measurement of heat of adsorption and surface area for the sensitive films of Al_2O_3 created using processes described above. The films were formed on ST-cut quartz^a SAW devices and the adsorption of ethanol (EtOH) was

^a ST-cut quartz is a singly rotated cut having Euler angles $\lambda = 0^\circ$, $\theta = 90^\circ$, and $\mu = 132.75^\circ$.

measured. The adsorption isotherms were then fit using the Marquardt-Levenberg algorithm to extract the values of the heat of adsorption of the first monolayer onto the surface and the limiting number of surface layers adsorbed.⁸ This information was then compared to published values for the heat of adsorption and the surface areas of the films was estimated and compared to the preparation conditions.

The BET adsorption model is a widely accepted technique for experimentally determining the surface area and heat of adsorption of the first monolayer of adsorbate onto a surface.⁷ BET measurements are routinely made with N₂ as the adsorbate on a surface cooled to 77 K and are used to study the properties of materials ranging from soils to sol-gels.⁹⁻¹¹ N₂ is the adsorbate of choice due to its well known adsorption cross section (16.2 Å²); however, typical instrumentation designed to make BET measurements is limited to bulk materials and does not allow for measurements of thin-film adsorption. The adsorption characteristics of a bulk material may or may not be representative of the adsorption characteristics of thin films made from that material. Previously, SAW technology has been used to make BET measurements of thin silicate-based sol-gel films by adsorbing N₂ in a He matrix onto a test film cooled to 77 K that was deposited on a SAW device.¹² We have used this technique at room temperature to measure the heat of adsorption and surface area of the Al₂O₃ films described in this paper.

The surface acoustic wave sensor system used to make the measurements was similar to the system reported previously.¹³ The system used six SAW devices, each with a different film; all were exposed to the same atmosphere of interest at the same time. Each SAW device was used as the feedback element of an oscillator circuit operating at approximately 97 MHz. The frequency outputs from the oscillators were then measured to 1 Hz resolution using a frequency counter (HP5385A). All SAW devices were mounted in a single brass test fixture whose temperature was actively controlled using a liquid flow from a temperature controlled bath (Haake model K). The brass fixture was designed to provide excellent radio frequency (rf) shielding for the test SAW devices and to provide sufficient thermal mass to moderate the frequency changes due to environmental temperature fluctuations.

The SAW device-based oscillators respond to the adsorption of a chemical species by changes in the wave propagation velocity of the film and this is observed as a change in the frequency of the oscillator. The mechanical influences that effect the frequency of a SAW sensor in an oscillating loop can be written as¹⁴

$$\frac{\Delta\nu}{\nu_0} = -k_m \frac{\Delta\rho}{\rho_0} + k_s \frac{\Delta S}{S_0} + k_\sigma \frac{\Delta\sigma_q}{\sigma_{q0}} + k_\gamma \frac{\Delta\gamma}{\gamma_0} - k_T \frac{\Delta T}{T_0} \quad [1]$$

where ν is the frequency of oscillation, ρ is the surface mass density of material on the surface of the SAW device, S is the modulus of elasticity of the ST-cut quartz, σ is the conductivity of the film, γ is the stress parameter in the sensing film, and T is the temperature of the SAW surface. The values of k are constants for each parameter of the equation, and the subscript 0 refers to the initial conditions of the unloaded sensor. For our films constructed from Al₂O₃ in a temperature controlled environment, the change in all terms except the surface mass density is approximately zero. Therefore, to first order, the wave velocity is reduced as material is adsorbed onto the surface of the device; the frequency change can be written as a function of surface mass change according to the following relationship¹²

$$\Delta\nu = -\eta_m \nu_0^2 \Delta\rho \quad [2]$$

where $\Delta\rho$ is the change in surface mass density due to the adsorption of the adsorbate onto the film, $\Delta\nu$ is the change in frequency due to the adsorbate, η_m is the mass sensitivity factor (1.3 × 10⁻⁶ cm²/g) of the ST-cut quartz substrate,¹⁵ and ν_0 is the base-line frequency of the SAW oscillator (~97 MHz).

Various concentrations of EtOH in N₂ were passed over the sensors and the frequencies were measured at a single temperature (20°C). These isothermal data are illustrated in Fig. 6 as a plot showing the change in the frequency between the initial frequency and the current frequency at a given concentration. The concentration is represented as the ratio between the partial pressure of the alcohol and that alcohol's saturation vapor pressure at the test temperature (20°C). The data points on the plot are the measured data and the solid line is a fit of the data to the modified BET experimental isotherm model. The modified BET model of chemical adsorption postulates that there are two heats of adsorption of the adsorbate onto the film: the larger heat of adsorption is that of the first monolayer binding to the film surface and the smaller heat of adsorption is that of the adsorbate binding to itself (*i.e.*, the heat of vaporization of the adsorbate). The modification of the BET from its initial form is the addition of the parameter n , which is the limiting number of monolayers that will adsorb onto the surface. The pore size or other physical limitations usually determine this limit. The standard BET model is limited in applicability to a concentration range of 0-30% P/P_{sat} where P is the partial pressure of the adsorbate and P_{sat} is the saturation vapor pressure of the adsorbate; however, the modified form has been shown to have a much greater range of applicability.⁸

It is apparent from Eq. 2 that the change in the number of molecules (ΔN) binding to a surface is proportional to the change in frequency of the SAW oscillator. Therefore, we may write the modified BET equation in terms of frequency changes rather than changes in the number of molecules as is commonly seen

$$\frac{\Delta\nu}{\Delta\nu_m} = \frac{\Delta N}{\Delta N_m} = \frac{c\xi}{(1-\xi)} \frac{1 - (n+1)\xi^n + n\xi^{n+1}}{1 + (c-1)\xi - c\xi^{n+1}} \quad [3]$$

where ξ is the ratio between the partial pressure of the adsorbate and its saturation vapor pressure (P/P_{sat}); $\Delta\nu$ is the frequency change due to the adsorbate at the current partial pressure; $\Delta\nu_m$ is the frequency change due to one monolayer coverage on the surface; c is a constant that depends on the difference in the heat of adsorption between the adsorbate and the surface (Q_1), the heat of vaporization of the adsorbate (Q_v), the temperature of the surface (T), and the universal gas constant (R)

$$c = e^{(Q_1 - Q_v)/RT} \quad [4]$$

The data were fit to Eq. 3 using a nonlinear Marquardt-Levenberg regression algorithm with three adjustable parameters: the monolayer coverage frequency change ($\Delta\nu_m$), the heat of adsorption constant (c), and the limiting number of monolayers adsorbed (n). The heat of adsorption of the first monolayer of EtOH onto Al₂O₃ was estimated from Eq. 4 to be 9.78 kcal/mol (the heat of vaporization for EtOH is approximately 9.67 kcal/mol¹⁶). The value for the heat of adsorption of EtOH compares favorably to the values found in the literature of 10.1 kcal/mol.¹⁷

From the single monolayer frequency change ($\Delta\nu_m$), it is possible to estimate the surface area of the film given convenient assumptions. We assume that EtOH is a spherical molecule with a standard area (A_{EtOH}) of 32.5 Å². This value was found by using the van der Waals constant for the volume occupied by 1 L of molecules and calculating the area. A similar calculation was performed on H₂O as a check of the validity of the method and the area was found to be consistent with the literature value for the standard area of H₂O. The area of the film can then be calculated from the following formula

$$A_{\text{film}} = \frac{-\Delta\nu_m A_v}{\nu_0^2 \eta (MW_{\text{EtOH}})} A_{\text{EtOH}} \quad [5]$$

where A_v is Avogadro's number and MW_{EtOH} is the molecular weight of ethanol (46 g/mol).

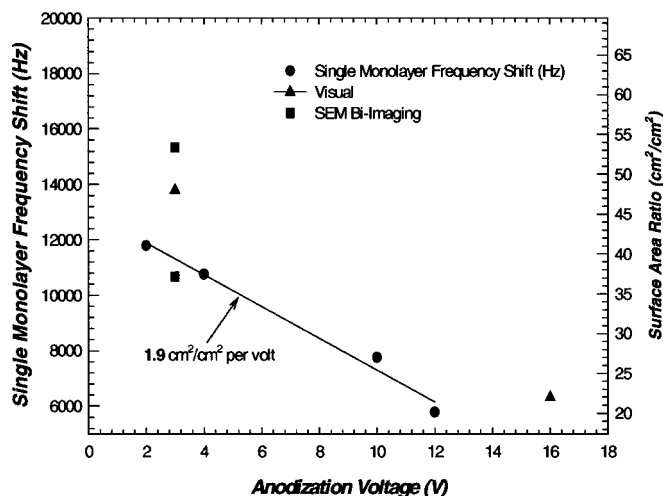


Figure 7. Plot of single layer frequency shift as a function of anodization voltage. The right-hand axis is scaled to provide the ratio of film surface area as a function of anodization voltage. (●) Indicates the SAW data. (■) Are data obtained from SEM bi-imaging measurements of similarly grown films. (▲) Are measurements made by visually examining SEM photographs of the films and calculating the surface area from the pore density, pore diameter, and known film thickness.

We have plotted the single monolayer frequency change as a function of anodization potential in Fig. 7. From these data, we can estimate the change in surface area as a function of anodization voltage. In addition, we have estimated that the film formed at 2 V anodization potential has a surface area of about 40 (cm²/cm²) and the surface area decreases at a rate of 1.9 (cm²/cm²) for each 1 V increase in potential. The nomenclature A (cm²/cm²) implies that for every 1 cm² of planar coverage, the film has A cm² of actual surface area. The surface areas of several similar films were measured using other techniques, including SEM bi-imaging and manually computing the surface area by measuring the pore diameter from an SEM image and assuming a cylindrical pore of known depth. Both of these techniques compare favorably with the BET technique as is clear from Fig. 7.

The parameter n has an average value of 19 layers for all of the films tested (Fig. 8). Our SEM measurements of pore size indicate that the pores of the samples tested are between 7 nm and 20 nm in diam for films in the 2 and 12 V range; the diameter of the spherical EtOH model is on the order of 0.64 nm. Thus, 19 monolayers of rigid spherical molecules will not fit in the pores. Thus, we might conclude that the packing density of the molecules is higher when packed into the pores increasing the average number of monolayers on the surface. However, the value of n is not critical to the calculation of the surface area since surface area is derived from the single monolayer coverage value. Thus, the surface area value reported is unaffected by this inconsistency in the modeled results.

Conclusion

Thus, we have illustrated the utility of a surface acoustic wave analysis of the surface area of thin films formed by anodizing metallic Al films that were deposited under greater surface mobility (zone II conditions). We have calculated the surface area and found that for every 1 V decrease in anodization potential the surface area of the film increased by 1.9 (cm²/cm²) over the range tested. This rate will not continue at either the lower or upper limits of potential; however, over this somewhat limited range of applicability the film grower can engineer the surface area to controllable values.

The general conclusion from this study suggests that complete film anodization under a low potentiostatic mode is reached near the end of the second stage. Continued exposure of the film in the acid

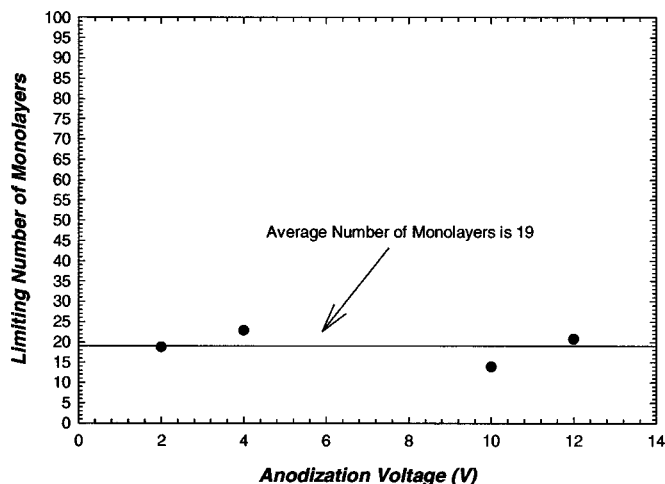


Figure 8. Plot of average number of monolayers that form on the surface of the films as determined from a fit of the data to the BET model. While the average value ($n = 19$) is inconsistent with the number that is calculated to fit in a pore (assuming a diam of 0.6 nm) as found from the spherical model, the results found for the surface area are calculated from the single monolayer response and are therefore, consistent.

electrolyte during the third stage only deteriorates the columnar morphology. In addition, we have measured the surface area of the films by measuring the adsorption isotherms of the films and extracting the surface area and heat of adsorption using the modified BET model of adsorption. The results indicate that the heat of adsorption of the first monolayer is 9.78 kcal/mol and the surface areas decrease over the values of potential tested at a rate of -1.9 (cm²/cm²)/V. This allows the film surface area to be engineered to a precise surface area as desired. These types of studies will allow further development of chemically sensitive films for application in detection, quantification, and speciation of unknown chemical plumes found in the environment.

Acknowledgment

Sandia is a multiprogram laboratory operated by Sandia Corporation, a Lockheed Martin Company, for the United States Department of Energy under contract DE-AC04-94AL85000.

Sandia National Laboratories assisted in meeting the publication costs of this article.

References

- A. J. Ricco, G. C. Osbourn, and R. M. Crooks, *Acc. Chem. Res.*, **31**, (1998).
- H. Asoh, K. Nishio, M. Nakao, T. Tamamura, and H. Masuda, *J. Electrochem. Soc.*, **148**, B152 (2001).
- J. P. O'Sullivan and G. C. Wood, *Proc. R. Soc. London*, **317**, (1970).
- C. Miller and M. Majda, *J. Electroanal. Chem.*, **207**, 49 (1986).
- B. A. Movchan and A. V. Demchishin, *Phys. Met. Metallogr.*, **28**, 83 (1969).
- S. Brunauer, P. H. Emmett, and E. Teller, *J. Am. Chem. Soc.*, **60**, 309 (1938).
- A. W. Adamson, *Physical Chemistry of Surfaces*, p. 538, John Wiley & Sons, New York (1982).
- K. B. Pfeifer, *Langmuir*, **11**, 4793 (1995).
- C. T. Chiou, *Environ. Sci. Technol.*, **24**, 1164 (1990).
- W. Wagner, R. S. Averback, H. Hahn, W. Petry, and A. Wiedenmann, *J. Mater. Res.*, **6**, 2193 (1991).
- R. Tsunoda, *J. Colloid Interface Sci.*, **130**, 1,60 (1989).
- A. J. Ricco, G. C. Frye, and S. J. Martin, *Langmuir*, **5**, 273 (1989).
- R. W. Cernosek, W. G. Yelton, C. W. Colburn, L. F. Anderson, A. W. Staton, G. C. Osbourn, J. W. Bartholomew, R. F. Martinez, A. J. Ricco, and R. M. Crooks, in *Chemical Microsensors and Applications II*, SPIE, Vol. 3857, p. 147 (1999).
- S. L. Hietala, Ph.D. Dissertation, University of New Mexico (1997).
- D. S. Ballantine, R. M. White, S. J. Martin, A. J. Ricco, E. T. Zellers, G. C. Frye, and H. Wohltjen, *Acoustic Wave Sensors: Theory, Design, and Physico-Chemical Applications*, p. 74, Academic Press, San Diego, CA (1996).
- Handbook of Chemistry and Physics*, 44th ed., p. 2412, CRC Press, Boca Raton, FL (1962).
- P. F. Rossi and P. Rossi, *Adsorption Sci. Technol.*, **13**, 215 (1996).